



Science Arts & Métiers (SAM)

is an open access repository that collects the work of Arts et Métiers Institute of Technology researchers and makes it freely available over the web where possible.

This is an author-deposited version published in: <https://sam.ensam.eu>
Handle ID: <http://hdl.handle.net/10985/10301>

To cite this version :

Amine MEHEL, Céline GABILLET, Henda DJERIDI - Analysis of the flow pattern modifications in a bubbly Couette-Taylor flow - Physics of Fluids - Vol. 19, p.118101-1: 118101-4 - 2007

Any correspondence concerning this service should be sent to the repository

Administrator : scienceouverte@ensam.eu



Analysis of the flow pattern modifications in a bubbly Couette-Taylor flow

A. Mehel, C. Gabillet,^{a)} and H. Djeridi^{b)}

IRENav, Institut de Recherche de l'Ecole Navale, Lanvéoc Poulmic, BP 600, 29240 Brest Armées, France

The aim of this Brief Communication is to discuss the bubble effect on the Couette-Taylor flow patterns in the transition from laminar to turbulent flow, especially in the weakly turbulent regime. It is shown that bubble location and local void fractions both in the vortices cores and in the near wall regions directly influence the axial wavelength. Bubbles trapped in the vortices tend to increase the vorticity and reduce the axial diffusivity. Bubbles near the wall contribute to "shear induced" turbulence depending on the void fraction gradient near the wall and the bubble size.

Studying flows between two coaxial circular cylinders is of much interest for chemical, biomedical, and nuclear applications. In this particular flow, increasing the rotation speed of the inner cylinder leads to the development of well known instabilities and turbulence takes place progressively. As far as the single-phase flow is concerned, the state of the art is very copious but very few studies deal with bubbly flow in this configuration.

Experimental studies have already been conducted in turbulent Couette-Taylor bubbly flows with superimposed axial flux.^{1,2} The arrangement of the bubbly phase depends on the ratio between the Taylor number Ta , characteristic of the rotation rate, and the Reynolds number, characteristic of the injection axial flux. Nevertheless, in this situation, the bubble effect on the flow patterns cannot be decoupled from the axial flow effect that tends to reduce the size of the Taylor vortices and thus the axial wavelength.

In order to investigate the interactions between bubbles and the flow structures, it is necessary to conduct studies without superimposed axial flow in the transition from laminar to turbulent flow. The question we try to answer is: What is the bubbles' location and the void fraction effect on the Taylor vortices intensity, the wall shear stress, and the transition to higher order instabilities? To this end, measurements were conducted in two complementary experimental devices detailed in Refs. 3–5.

Detailed results obtained for the wavy vortex flow and modulated wavy vortex flow regimes ($188 < Ta < 543$) are discussed in depth in Ref. 3. It is put into evidence that millimetric vapor bubbles generated by pressure drop (cavitation) are periodically arranged. They are located either in the Taylor vortices for $Ta < 300$ or in the outflow regions for larger Taylor number. In this latter situation, there is an increase in the axial wavelength and a premature transition to the third instability induced by the migration of the bubbles in the outflow regions.

However, in order to investigate the correlation between the flow pattern modifications and the local dispersed phase

characteristics (void fraction, bubble size, and drift velocity), a larger experiment was built that makes it possible to introduce a dual fiber-optic probe and to perform measurements for higher instabilities. In Ref. 4, void fraction and velocity profiles measured in this new experimental device are presented and discussed according to the bubble size: millimetric bubbles (cavitation) or submillimetric bubbles (ventilation). In Ref. 5, further measurements obtained for millimetric bubbles with another ventilation procedure are displayed. The changes in the flow patterns are obviously more pronounced when the bubble size is increased. The objective of the present Brief Communication is to summarize and bring together results obtained in weakly turbulent flow for millimetric bubbles by the way of different procedures.^{4,5} It gives an extended analysis of modifications in axial wavelength, vorticity, wall shear stress, and diffusivity, as a function of local phase characteristics, through a dimensional approach.

The geometry of the experimental device is characterized by the following nondimensional parameters (gap: $d/R_i = 0.1$; height: $\Gamma = L/d = 40$) with $d = R_o - R_i = 20$ mm. The Taylor number is defined as $Ta = \sqrt{\Omega_i R_i d^3 / \nu^2}$, where Ω_i is the inner cylinder angular velocity, R_i the radius, and ν the viscosity of the experimental fluid, which is a mixture of water and glycerol. Figure 1 shows a general schematics of the apparatus. The characteristics of the single-phase flow patterns are given in Ref. 4. In this study, special attention was paid to the quasiperiodic regime at $Ta = 780$, and the weakly turbulent regime at $Ta = 1000$. From now on, subscript "0" is used to denominate the single-phase flow patterns.

The bubbles were generated either by air injection at the bottom of the apparatus associated with a pressure drop (gaseous cavitation) or by ventilation at the upper free surface. The bubble size depends on the generation procedure: millimetric bubbles for cavitating flows, both millimetric and submillimetric bubbles for ventilated flows (denoted "CF" and "VF," respectively). The ventilation procedure is slightly different than the one used in Ref. 4, where only submillimetric bubbles were trapped in the gap.

For CF and VF, millimetric bubbles are localized both in the outflow regions near the inner cylinder and in one in two

^{a)}Electronic mail: gabillet@ecole-navale.fr

^{b)}Present address: Laboratoire de Physique des Océans, 6 Avenue Le Gorgeu, B.P. 809, 29285 Brest Cedex, France.

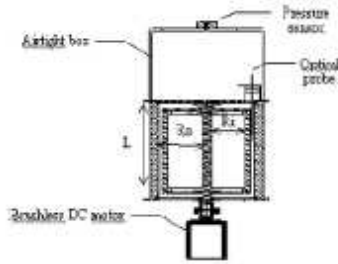


FIG. 1. General schematics of the apparatus.

Taylor vortex cores, as can be seen in Fig. 2. In the vortex cores, millimetric bubbles of size $d_B/d=0.16-0.18$ are spherical shaped. In the outflow region, millimetric bubbles are elongated in the direction of the azimuthal flow (large axis of the ellipsoid $l_{BB}/d \approx 0.3$). For the ventilated flow, the obtained submillimetric bubbles ($d_B/d=0.04$) are localized in the outflow regions. In Table I, contribution of millimetric and submillimetric bubbles to the void fraction are distinguished by a special treatment of the optical probe signal.⁵ It is necessary to discriminate the respective contributions in order to analyze specific effect of millimetric bubbles on the flow patterns. The axial wavelength can be linearly stratified (SF) or homogeneous (HF), according to the bubble generation procedure. For cavitation, the flow is stratified during the pressure decrease and reorganizes into a homogeneous flow as soon as pressure is stabilized. For ventilation, the flow remains stratified. Local measurements were performed in the third bubble string below the free surface. The void fraction α , bubble size d_B , and azimuthal velocity V_B were determined with a dual fiber-optic probe. The liquid azimuthal and axial velocity components (v, w) were characterized by laser Doppler velocimetry.

Figure 3 shows that the relative variation in the axial wavelength evolves linearly with the difference between the void fraction in the vortices core and the void fraction in the outflow region near the inner cylinder. As was suggested in Ref. 4, it is now obvious that bubbles located preferentially in the vortices' core tend to reduce the vortex size, whereas bubbles located preferentially in the outflow region tend to increase this size.

Let us now suggest the physical understanding. To achieve this, it is necessary to have a look at the bubbles'

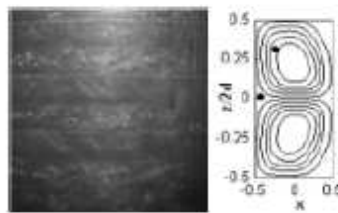


FIG. 2. Visualization of the bubble arrangement for the homogeneous cavitating flow [x denotes the normalized radial position $x=r/d-(Ri/d+0.5)$].

TABLE I. Bubble contribution to the void fraction and wall shear stress. (void fraction gradient and bubble drift velocity are determined at $x=-0.375$ in the third bubble string below the free surface, n_B is the bubble string number in the gap).

	Ta	Flow	α (%)	$\alpha_{\text{millimetric}}$ (%)	$\frac{V_0 - V_B}{V_0}$	$\frac{\tau_W - \tau_{W0}}{\rho \nu V_0/d}$
	Ω (rps)	pattern	core			
CF	780	$n_B=15$				
	1.56	SF	0.35	0.077	0.28	0.65
		HF	0.12	0.045	0.28	0.38
	1000	$n_B=16$				
VF	1.76	SF	0.75	0.139	0.26	0.81
		HF	0.3	0.07	0.21	0.41
	780	$n_B=14$		millimetric:		
	3.07	SF	0.21	0.062	0.24	0.33
				submillimetric:		
				0.21		
	1000	$n_B=14$		millimetric:		
	3.07	SF	0.23	0.079	0.19	0.27
				submillimetric:		
				0.36		

effect on the vorticity when bubbles are trapped in the vortices. Values of the local pressure Laplacian can be used to distinguish "vorticity dominated" regions (positive values) from "strain dominated" regions (negative values). To calculate the pressure Laplacian, an analytical solution for the velocity field must be known. For this purpose, a fourth-order Fourier decomposition (Davey's expansion theory extended to larger Taylor numbers⁶), applied to axial profiles of measured values of axial and azimuthal mean velocity components, was achieved. Davey's coefficients were then radially fitted by polynomial curves. The mean radial velocity u was deduced from the continuous equation. Errors induced by this decomposition are deduced from comparison between experimental and analytical data. Relative errors are less than 5% and 2% for axial and azimuthal velocities, respectively.

Figure 4 displays the isocontours of pressure Laplacian for single and cavitating flows at $Ta=780$. With the presence of the bubbles, the global vorticity increases and the location of the global maximum shifts towards the inner cylinder and farther from the outflow region. This is in agreement with the capture of the bubbles at the position $(z/\lambda=0.34, x=r/d-(Ri/d+0.5)=-0.22)$, as can be seen in Fig. 2) which tends to augment the local vorticity, with a reinforcement in the inflow and a reduction in the outflow of the shear between the vortices. The buoyancy leads to an upward shift of the vortex core. Let us consider the final location of the bubbles in the

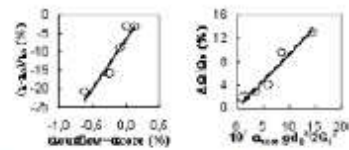


FIG. 3. Relative variation in axial wavelength and vorticity induced by the bubbles as a function of void fraction due to millimetric bubbles and normalized momentum exchange, respectively.

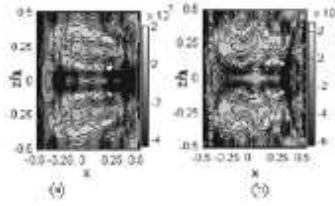


FIG. 4. Pressure Laplacian obtained by modelization of the velocity field at $Ta=780$: (a) single-phase flow and (b) homogeneous cavitating flow.

vortex r_{eq} , with G and R the vortex strength and radius. A dimensionless analysis shows that r_{eq}/R depends on three parameters such as $(d_B/R, d_B^3 g/G^2, Re_B = Gd_B/\nu R)$. The second parameter is the ratio between buoyancy and inertia effects, Re_B is the ratio between inertia and viscous effects. In the present study d_B/R and Re_B are quite constant (equal to $0.21 \pm 5\%$ and $52 \pm 15\%$, respectively). Assuming that the bubble drift velocity at the equilibrium position can be deduced from the vortex strength, the ratio $6C_d g_{eq}/8d_B$ representative of the ratio between drag force and inertia forces (lift, tchen, and added mass) applied to the bubbles is of order 1. C_d is the drag coefficient deduced from Moore's correlation.⁷ When we consider the balance between the forces including buoyancy, it can be shown that r_{eq}/R evolves as $g d_B^3/G^2$, in agreement with a shift of the final location outward according to the ratio between buoyancy and inertia. r_{eq} obviously augments when bubble diameter increases or vortex strength decreases. The force by unit volume induced by the bubbles trapped in the vortex ΔF_b is the consequence of added mass, lift, and drag forces and evolves as $\alpha_{core} \rho G^2 r_{eq}/4\pi^2 R^4$. Hence, the bubbles lead to an increase in the pressure gradient that can be normalized by the global initial pressure gradient. When considering the formulation of r_{eq}/R , it yields

$$2 \frac{\Delta \Omega}{\Omega_0} = \frac{\Delta(\text{grad } P)}{(\text{grad } P)_0} = \frac{\Delta F_b}{(\text{grad } P)_0} \approx \alpha_{core} \frac{g d_B^3}{G^2}. \quad (1)$$

The bubble induced relative vorticity is now determined assuming that $\Delta \Omega/\Omega_0 = \Delta v_t/v_{t0} - \Delta \lambda/\lambda_0$, where v_t is the tangential velocity deduced from the measurement of mean axial velocity profiles at the radial position $x=0.25$. The evolution of bubble induced vorticity with respect to $\Delta F_b/(\text{grad } P)_0$ is plotted in Fig. 3. It is interesting to note that the vorticity expands almost linearly with the void fraction in the core and the ratio between buoyancy and inertia. The bubble capture in the core is responsible for an increase in vorticity and pressure gradients in order to compensate for bubble buoyancy. This is in agreement with a reduction in the vortex size, depending on the bubble residence time and the bubble number in the vortex, as was expected by Gopalan and Katz.⁸

When submillimetric bubbles are localized in the outflow region near the inner cylinder, there is an increase in the axial wavelength, associated with a decrease in the vorticity of the vortices (ventilated flow at the bottom of the apparatus). Nevertheless, when millimetric bubbles are trapped in

the outflow region, the increase in the vortex size can be balanced by the augmentation of vorticity due to bubble capture in the core of the vortices (top of the apparatus in cavitating and ventilated flows).

In the single-phase Couette-Taylor flow, the increase in the axial wavelength is observed when turbulence develops and it is linked to the increase in the wall shear stress.⁹ This conjecture is worth being checked in two-phase flow by analyzing the velocity gradient of the liquid near the wall in the outflow region. In Refs. 4 and 5, it is shown that in this region, bubbles move slower than the liquid in the azimuthal direction. This is due to their migration process, which makes them move from the opposite side of the gap towards the inner rotating cylinder. Therefore, the azimuthal bubble drift velocity $(V_B - V)$ leads to a decrease in the mean azimuthal velocity of the liquid near the inner cylinder $\Delta V/V_0$.

Let us now consider a simple model that correlates $(V_B - V)$ and ΔV . Based on a "two-fluid" approach, the change in the azimuthal momentum is due mainly to the bubble induced momentum associated with drag effects of millimetric bubbles. Under these considerations, the azimuthal liquid velocity is deduced from the following expression:

$$V \approx V_0 + \frac{3k_B \nu r}{4d_B^2 U_0} \alpha_B (V_B - V_0), \quad (2)$$

where α_B is the contribution of millimetric bubbles to the void fraction, k_B is the ratio between the drag coefficient and the bubble Reynolds number $(|V_B - V_0|d_B/\nu)$, and can be determined with Moore's correlation.⁷ V_0 and U_0 are referred here to the mean azimuthal and radial velocity components of the undisturbed flow (i.e., the single-phase flow). For the bubble Reynolds number at stake (≈ 85), had we taken into account for interface contamination, the drag coefficient¹⁰ would have been greater by a factor $C \approx 2$. Another issue is that we have to consider the contribution of the bubble induced velocity gradient in the azimuthal momentum exchange:

$$\frac{\Delta V}{V_0} + \frac{r}{V_0} \Delta \left(\frac{\partial V}{\partial r} \right) \approx C \frac{3k_B \nu r}{4d_B^2 U_0} \alpha_B \left(\frac{V_B - V_0}{V_0} \right).$$

Near the inner cylinder, at $x=-0.375$, experimental data⁴ show that

$$\frac{r}{V_0} \Delta \left(\frac{\partial V}{\partial r} \right) \approx -0.7 \Delta \left(\frac{\Delta V}{V_0} \right).$$

With this approximation, the bubble induced azimuthal velocity can be expressed as

$$\frac{\Delta V}{V_0} \approx \frac{1}{1 - 0.7 C \frac{3k_B \nu r}{4d_B^2 U_0} \alpha_B} \frac{(V_B - V_0)}{V_0}.$$

The validity of the "two-fluid" approach can be checked in Fig. 5. $\Delta V/V_0$ near the inner cylinder deduced from experimental data at $x=-0.375$ shows a quite linear correlation with respect to $\alpha_B(V_B - V_0)/V_0$, the slope being ten times as great as

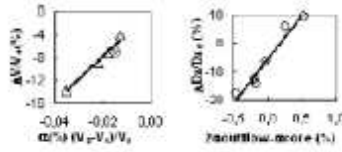


FIG. 5. Relative variation in mean azimuthal velocity and axial diffusivity induced by the bubbles as a function of void fraction and drift velocity, near the wall in the outflow. (\diamond — \diamond) Ventilated flows; (\triangle — \triangle) cavitating flows; (\circ — \circ) all flows.

$$\frac{3k_g}{4d_B^2} \frac{\nu r}{U_0} \frac{(V_B - V_0)}{V_0}.$$

As expected from this, the shear stress can be written as

$$\tau_{\theta\theta}(r) = \tau_{\theta\theta 0} + 10 \frac{3k_g}{4d_B^2} \frac{\nu r}{U_0} \mu \times \left[\alpha_B \frac{V_B - V_0}{r} - \alpha_B \frac{\partial(V_B - V_0)}{\partial r} - \frac{\partial \alpha_B}{\partial r} (V_B - V_0) \right].$$

The wall is expected to play a repellent role for the bubbles;¹¹ the void fraction at the inner cylinder wall is thus considered as negligible, whereas the radial gradient of the void fraction has a significant positive value. The expression of the wall shear stress yields

$$\tau_w = \tau_{w0} - 10 \frac{3k_g}{4d_B^2} \frac{\nu R_i}{U_0} \mu (V_B - V_0) \frac{\partial \alpha_B}{\partial r} \Big|_{r=R_i}. \quad (3)$$

Taking into account that the bubble velocity is less important than the liquid velocity near the inner wall, the wall shear stress appears to be greater than the one obtained in single-phase flow. Thus, a higher value of the void fraction near the inner cylinder is expected to lead to an increase in the shear stress. The “bubble induced” wall shear stress determined in the outflow from Eq. (3) is reported in Table I. Note that it is underestimated in ventilated flow because the contribution of submillimetric bubbles is expected to play a role in the very near wall region.

The bubble induced wall shear stress contributes to increase the production of turbulence near the wall. For the axial velocity component, additional turbulent kinetic energy was observed in the entire gap.⁵ As it has been shown in single-phase flow,¹² that the turbulent axial diffusivity D_z expands linearly with the axial wavelength, the relative variation in diffusivity can thus be roughly estimated following

$$\frac{\Delta D_z}{D_{z0}} = \frac{\Delta \lambda}{\lambda_0} + \frac{\Delta w_{rms}}{w_{rms 0}}.$$

w_{rms} is the rms axial velocity component measured near the inner cylinder in the outflow region. $\Delta D_z/D_{z0}$ is displayed in

Fig. 5 as a function of both the global void fraction in the outflow and the void fraction in the core of the vortices. It can be seen that the diffusivity is proportional to $(2\alpha_{outflow} - \alpha_{core})$, in agreement with a quasilinear growth of w_{rms} with $\alpha_{outflow}$ or $(\partial \alpha / \partial r)_{R_i}$ in the outflow and a linear dependence of λ with $(\alpha_{outflow} - \alpha_{core})$. Hence, bubbles localized near the wall in the outflow region are supposed to increase the axial diffusivity, whereas bubbles captured inside the Taylor vortices are expected to reduce this quantity.

To conclude this Brief Communication, for the bubbly Taylor-Couette flow in the quasiperiodic and in the weakly turbulent regimes, it is demonstrated that modifications in the flow patterns depend on the bubble location in the gap, according to their size and that they are correlated with the local void fraction. For bubbles located near the wall, drift velocity is responsible for the homogenization of azimuthal momentum in the gap and the increase in the wall shear stress. This is in agreement with results expected in flows where bubbles injected outside the boundary layer bring closer to the wall and exhibit a void fraction peak. As a conclusion, bubbles localized in the outflow region contribute to increase the axial wavelength and to develop turbulence by shear induced turbulence. On the contrary, bubbles trapped in the core of the Taylor vortices are expected to stabilize the flow and increase the vorticity.

¹Y. Shiomi, H. Kutsuna, K. Akagawa, and M. Ozawa, “Two-phase flow in an annulus with a rotating inner cylinder (flow pattern in bubbly flow region),” *Nucl. Eng. Des.* **141**, 27 (1993).

²K. Aikhen, J. Fontaine, and J. E. Wesfreid, “Highly turbulent Couette-Taylor bubbly flow patterns,” *J. Fluid Mech.* **422**, 55 (2000).

³H. Djeridi, C. Gabillet, and J. Y. Billard, “Two-phase Couette-Taylor flow: Arrangement of the dispersed phase and effects on the flow structures,” *Phys. Fluids* **16**, 128 (2004).

⁴A. Mehel, C. Gabillet, and H. Djeridi, “Bubble effect on the structures of weakly turbulent Couette-Taylor flow,” *J. Fluids Eng.* **128**, 819 (2006).

⁵A. Mehel, “Etude expérimentale d’un écoulement diphasique de Taylor-Couette,” Ph.D. thesis, Ecole Centrale de Nantes and Université de Nantes, 2006.

⁶A. Duvey, R. C. Di Prima, and J. T. Stuart, “On the stability of Taylor vortices,” *J. Fluid Mech.* **31**, 17 (1968).

⁷D. W. Moore, “The boundary layer on a spherical gas bubble,” *J. Fluid Mech.* **16**, 161 (1963).

⁸S. Gopalan and J. Katz, “Effect of entrained bubbles on the structure of vortex rings,” *J. Fluid Mech.* **397**, 171 (1999).

⁹G. Cognet, “Les étapes vers la turbulence dans l’écoulement de Taylor-Couette entre cylindres coaxiaux,” *J. Mec. Theor. Appl.*, special issue, p. 7 (1984).

¹⁰T. Maxworthy, C. Gnan, M. Körtgen, and F. Durst, “Experiments on the rise of air bubbles in clean viscous liquid,” *J. Fluid Mech.* **321**, 421 (1996).

¹¹D. Legendre and J. Magnaudet, “The lift force on a spherical bubble in a viscous linear shear flow,” *J. Fluid Mech.* **368**, 81 (1998).

¹²W. Y. Tam and H. L. Swinney, “Mass transport in turbulent Couette-Taylor flow,” *Phys. Rev. A* **36**, 1374 (1987).